JOURNAL OF GEOPHYSICAL RESEARCH, VOL. 91, NO. B12, PAGES 12,651–12,660, NOVEMBER 10, 1986

#7

Analysis of Borehole Seismograms From Long Valley, California: Implications for Caldera Structure

GREGORY J. ELBRING AND JOHN B. RUNDLE

Geophysics Division, Sandia National Laboratories, Albuquerque, New Mexico

A three-component seismometer was emplaced in a borehole in Long Valley caldera for a period of 2 months to record local earthquakes to the south, mostly in the Sierra Nevada. The seismic records were plotted in depth versus time sections to produce "vertical hypocentral profiles" for both the vertical and horizontal components. The data collected and displayed in this way provide good resolution of the crustal structure at depth and avoid the attenuation and complications introduced by the near-surface caldera fill. The record sections were then modeled with two-dimensional ray tracing to match the observed travel times. Although nonreversal of the profiles and uncertainties in hypocentral locations introduce ambiguities, the final interpretation reveals two separate low-velocity bodies which we have tentatively identified as magma beneath the resurgent dome in Long Valley. The first of these is a small (2 km by 6 km) body with a depth to top of approximately 3.7 km beneath the surface at the southern end of the resurgent dome. The other body appears larger and lies at a depth of 5.5 km beneath the northern end of the resurgent dome.

INTRODUCTION

The search for and consequent examination of crustal magma bodies by conventional seismic methods often encounter difficulty due to the complex surface structure typical of volcanic regions. New techniques of data acquisition and analysis need to be combined with conventional techniques to define more fully and accurately the crustal structure in such regions.

An obvious way to improve data quality is to place both the seismic source and receiver below as much of the complicated surface structure as possible, thereby eliminating unwanted multiples created by near-surface layers and avoiding the more attenuating sections of the ray path. To do this, we recorded microearthquakes in the vicinity of Long Valley caldera using a three-component seismometer emplaced in a borehole near the center of the caldera at 900 m depth within the Bishop Tuff [*Rundle et al.*, 1985]. Using events recorded from similar azimuths but a variety of depths, a depth versus time section or "vertical hypocentral profile" (VHP) was created for both the compressional and shear wave arrivals. These sections were then modeled with two-dimensional ray tracing to obtain a model of the deeper structure beneath the caldera.

PREVIOUS WORK

Volcanism in the Long Valley region began with the eruption of basalts about 3.2 Ma [*Bailey et al.*, 1976]. Subsequent eruptive events became progressively more rhyolitic, culminating in the caldera-forming Bishop Tuff eruption some 0.7 Ma. Since that time, numerous smaller eruptions have continued within the caldera along with the formation of a resurgent dome in the west central part of the caldera (see Figure 1). The history of volcanism continues into recent times with the eruption of the chain of Inyo Domes approximately 500 years ago. Moreover, since 1979 alone, there have been at least eight earthquakes in excess of magnitude 5 within and around the caldera, uplift of more than 0.5 m centered on the old resurgent dome, and rates of extension in the south central part of the caldera of several parts per million per year [*Hill et al.*, 1985*a*, *b*]. With the long history of eruptive events and the very recent activity, the possibility of locating shallow magma bodies within Long Valley has generated a great deal of interest.

A large number of geophysical studies have focused on Long Valley; *Rundle et al.* [1986] give an overview. Of particular interest to this work are the seismic surveys performed employing both conventional methods (i.e., reflection and refraction surveys) as well as more experimental and state-of-the-art techniques.

Refraction studies by *Hill* [1976] and *Hill et al.* [1985*c*] helped to define the intracaldera structure. Reflectors were identified beneath the northern end of the resurgent dome at estimated depths of about 7 km. *P* wave reflection surveys [*Rundle et al.*, 1985; *Deemer et al.*, 1985; *Deemer*, 1985] have helped to map out the uppermost few kilometers of the crust within the caldera, as well as identifying some deeper reflections beneath the northern part of the central resurgent dome, that might correspond to reflections from the top and bottom of a contemporary magma chamber. Recent *P* wave reflection work by *Murphy et al.* [1985] has also identified a deeper reflector beneath the southern end of the resurgent dome.

The high level of seismicity within the caldera and in the Sierra Nevada to the south has prompted a large number of investigations which use the earthquakes as sources. One of the more detailed studies was done by *Sanders* [1984], who defined two probable zones of magma beneath the caldera by studying shear wave extinction patterns for over 1200 ray paths through the caldera. Locations of these bodies are beneath the northwestern edge of the resurgent dome (a depth to top of about 5.5 km) and another shallower body (at 4.5 km depth to top) beneath the southeastern portion of the resurgent dome. These anomalous regions were thought to be cupolas on the surface of a single large magma body. *S* wave attenuation was also observed by *Ryall and Ryall* [1981] for a zone underlying the southern part of the resurgent dome and the south moat region of the caldera. Finally, *P* wave tomography [*Kissling et al.*, 1984] and teleseismic

Paper number 6B6031.
0148-0227/86/006B-6031$05.00

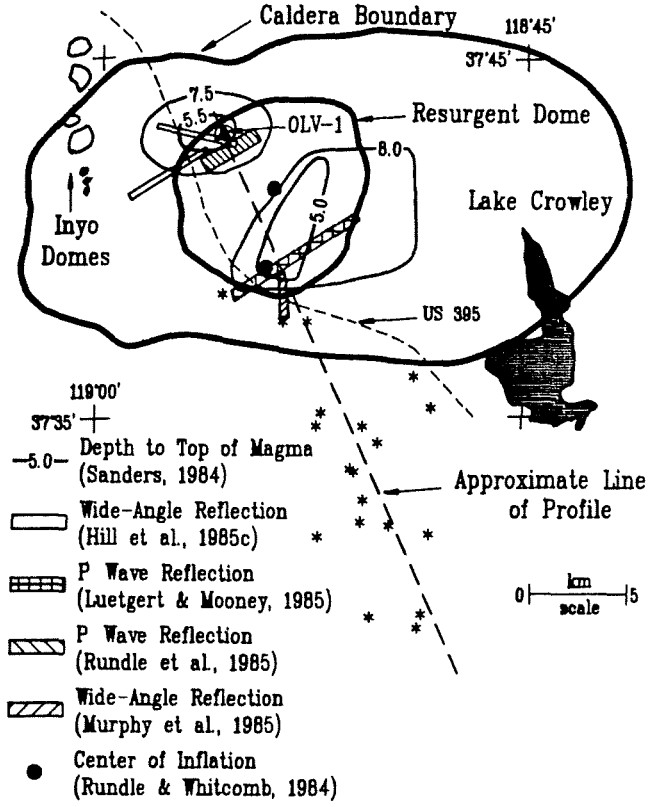

Fig. 1. Map of Long Valley region showing major physiographic features and subsurface features defined by several previous studies. Locations of well OLV-1 and earthquakes (asterisks) used in the present study are also indicated. Heavy dashed line shows orientation of cross section in Figures 4–6 and Figure 8.

delays [*Steeples and Iyer*, 1976] both indicated a small decrease in compressional velocities beneath the caldera.

In their attempt to image the deeper crust, most of the preceding seismic studies were limited by the attenuation and ray path complexity introduced by the near-surface caldera fill. To date, it has been somewhat difficult to obtain a good resolution of the detailed configuration of shallow magma within the caldera. On the one hand, avoiding the seismically attenuating and dispersive caldera fill implies long source-receiver offsets, relatively longer periods, and poorer depth resolution. On the other hand, improved depth resolution needs both source and receiver at closer offsets within the caldera, but with both source and receiver at the surface, the caldera fill severely attenuates, delays, and disperses the energy. Recognition of these problems led us to the design of the present experiment.

TECHNIQUE

We decided to record seismic energy from local earthquakes using a receiver in a geothermal well at the northern end of the resurgent dome, thereby placing both source and receiver below the worst effects of the caldera fill. Permission was subsequently obtained to reenter a 900-m-deep well (OLV-1) drilled by Santa Fe Geothermal, Inc., and a three-component, 8.0-Hz geophone was implanted at the bottom of the well in September 1984. At the same time, 4.5-Hz sensors with comparable higher-frequency responses were placed at the surface near the borehole, and at three other locations within 2 km, to compare the differences between the surface and borehole signals for the same events.

Earthquakes occurring in the Sierra Nevada south of the caldera were recorded digitally for a period of two months in September and October 1984. The events were recorded at a sampling rate of 100 samples per second on Sprengnether DR-100s with a standard 30-Hz low-pass Butterworth filter. Of the earthquakes recorded, a total of 19 events were deemed to have accurate timing and to be of sufficient depth variation for the purposes of our study. Also, these events were restricted to those with azimuths between 130° and 180° from the well location. This restriction focused the study on the area of greatest interest, the southern part of the resurgent dome, and was the only azimuthal range with a significant number of events during the monitoring period.

Hypocentral locations and origin times (see Table 1 and Figures 1 and 6) of these events were obtained from the U.S.

TABLE 1. Summary of Earthquake Origin Times, Locations, and Associated Errors

Date	Origin Time, UT	Latitude, °N	Longitude, °W	Depth, km	ERH,* km	ERZ,† km	rms,‡ s	Gap,§ deg
Sept. 21, 1984	1346:19.66	37.573	118.835	15.02	0.4	0.5	0.07	107
Sept. 27, 1984	2214:45.19	37.535	118.828	8.53	1.1	1.1	0.11	184
Sept. 27, 1984	2241:13.41	37.560	118.848	11.63	0.4	0.5	0.08	117
Sept. 28, 1984	0150:00.63	37.581	118.870	7.64	0.6	0.9	0.12	135
Sept. 28, 1984	0313:06.91	37.537	118.844	8.01	0.8	0.9	0.14	177
Sept. 28, 1984	0532:19.11	37.530	118.869	7.33	0.3	0.5	0.03	187
Sept. 28, 1984	0924:07.98	37.604	118.814	2.69	0.7	1.1	0.17	94
Sept. 28, 1984	1551:54.21	37.562	118.850	12.87	0.8	1.2	0.16	96
Sept. 28, 1984	2119:20.18	37.590	118.803	6.86	0.5	1.4	0.09	88
Sept. 29, 1984	0454:35.42	37.581	118.844	5.78	0.1	0.1	0.01	162
Sept. 29, 1984	0515:17.66	37.642	118.927	4.72	0.1	0.1	0.01	184
Sept. 30, 1984	0103:05.96	37.628	118.877	10.18	0.9	1.5	0.06	112
Sept. 30, 1984	0240:30.26	37.488	118.810	8.74	0.3	0.4	.0.05	156
Sept. 30, 1984	1057:22.65	37.493	118.837	11.59	0.8	1.0	0.04	200
Oct. 4, 1984	1033:27.40	37.494	118.808	9.66	0.6	0.7	0.05	173
Oct. 4, 1984	1122:48.28	37.587	118.868	8.17	0.2	0.2	0.02	126
Oct. 4, 1984	1738:34.62	37.547	118.843	10.41	0.8	1.3	0.11	94
Oct. 6, 1984	0855:59.70	37.532	118.803	13.96	0.4	0.7	0.04	143
Oct. 6, 1984	1250:51.70	37.629	118.891	5.56	0.4	0.6	0.09	112

* Standard error of the epicenter.
† Standard error of the focal depth.
‡ Root-mean-square error of the time residuals.
§ Largest azimuthal separation between stations recording earthquake.

Geological Survey (USGS) permanent stations in the region using the computer code HYPO71 [*Lee and Lahr*, 1975]. The accuracy of these values, especially the hypocentral depth, is an important factor in the analysis, and the effect on the final result will be discussed later.

The importance of having the sensor below most of the caldera fill is clearly illustrated in Figure 2, which compares the seismograms for two events recorded on both the downhole and surface instruments. These traces have been normalized to the frequency response of the 8.0-Hz geophone to remove the difference between the 8.0-Hz geophone downhole and the 4.5-Hz geophone at the surface. Little change arose from the normalization in the dominant frequency range of about 10–15 Hz.

For the vertical component the first arrival is obvious on all traces, but the frequency content of the downhole records is much higher. The difference is even more obvious on the horizontal component, where for the event on September 23, the downhole record shows a sharp shear wave arrival at approximately 0.1 s reduced time, which is virtually undetectable on the surface seismogram. For the September 27 event, the shear wave is present on the surface record, but the onset is much more emergent than on the downhole trace.

The individual signals were then plotted as depth versus time sections, with the vertical component plotted with a reducing velocity of 6.00 km/s and the horizontal components plotted with a reducing velocity of 3.35 km/s. In all cases, the distance used with the reducing velocity was the slant distance from the well to the hypocentral location. These record sections, called "vertical hypocentral profiles" (VHPs) relate to vertical seismic profiles (VSP) in much the same way as wide-angle refraction profiles relate to normal-incidence reflection profiles, in that VHPs and refraction sections are dealing with large angles of incidence, whereas VSPs and reflection work both deal with near-vertical travel paths. These VHPs contain a wealth of information about both the compressional and shear velocity structures of the area.

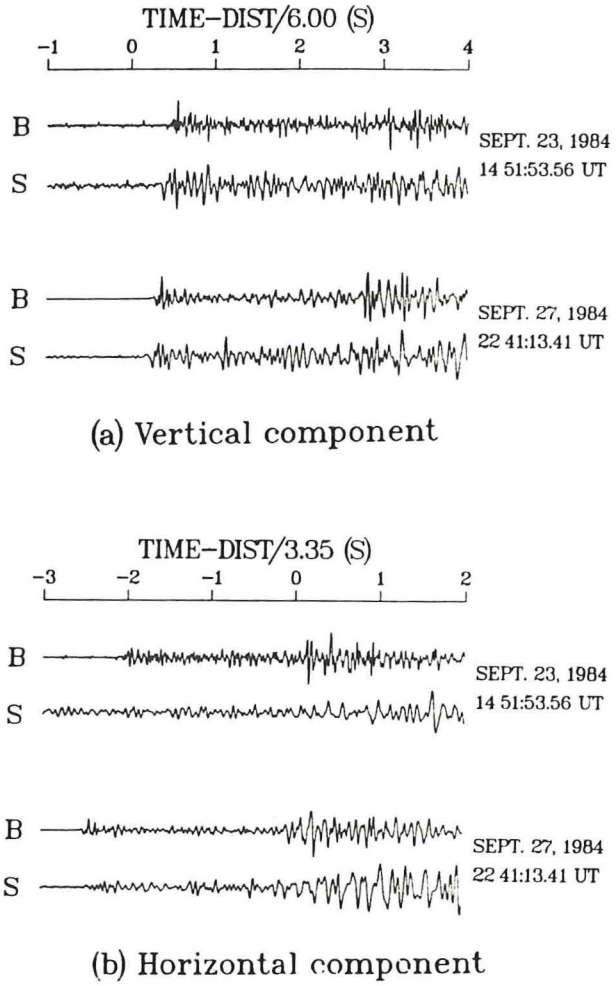

Fig. 2. Comparison of borehole (B) and surface (S) seismograms for both the (*a*) vertical and (*b*) one horizontal component.

MODELING

The VHPs created from the data recorded in Long Valley are shown in Figure 3. Seismograms are plotted with trace-normalized amplitudes since the different sources and azimuths for each trace mask the amplitude information contained in the records. The depth distribution of the sources provides a fairly continuous picture for depths between 5 and 15 km but is somewhat more ambiguous at shallower depths. The lack of hypocenters below 15 km prevented any modeling of the crust beyond this depth.

Modeling of the travel times displayed in the record sections was performed by iterative trial-and-error forward modeling using a modified version of the two-dimensional ray-tracing code from the technique developed by *Cerveny et al.* [1977]. Upper crustal structure, which could not be modeled by the present data set, was taken from the refraction results of *Hill et al.* [1985*c*]. No corrections were made for variations in the azimuth of the events, but variations in distance were accounted for by tracing rays to the appropriate epicentral distance at the corresponding focal depth. For ease of modeling, rays were traced from receiver to source giving correct travel times via reciprocity. We estimate that 99% of the data are fit to within ±0.1 s with 90% of the data fit to better than ±0.05 s. There were no data fits worse than ±0.2 s.

P Wave Velocity Model

In examining the vertical component record section first (Figure 3*a*), several important features are readily apparent. The most obvious is the delay of the first arrivals below about 7 km depth. For the reduced time plot and the expected compressional crustal velocity of roughly 6.0 km/s, the first arrival should come in at about 0 s, as it does between 5 and 7 km. Below 7 km, however, the arrivals are consistently delayed by as much as 0.4 s. Another principal feature is the secondary arrival about 0.3 s behind the first arrival. This was initially thought to be a multiple, but because the temporal separation between the two arrivals appears to decrease at depth, this event is probably a reflection rather than a multiple. A final feature is the change in slope of the arrivals between 7 and 8.5 km. Here again the arrivals are delayed beyond their expected arrival times.

A number of models were tried to examine the effects of low-velocity bodies of various sizes, shapes, and locations to explain the observed delays, with reflectors at various depths and orientations to match the observed reflected phase. The final model chosen to give the best fit to the data is shown in Figure 4 along with the vertical component VHP

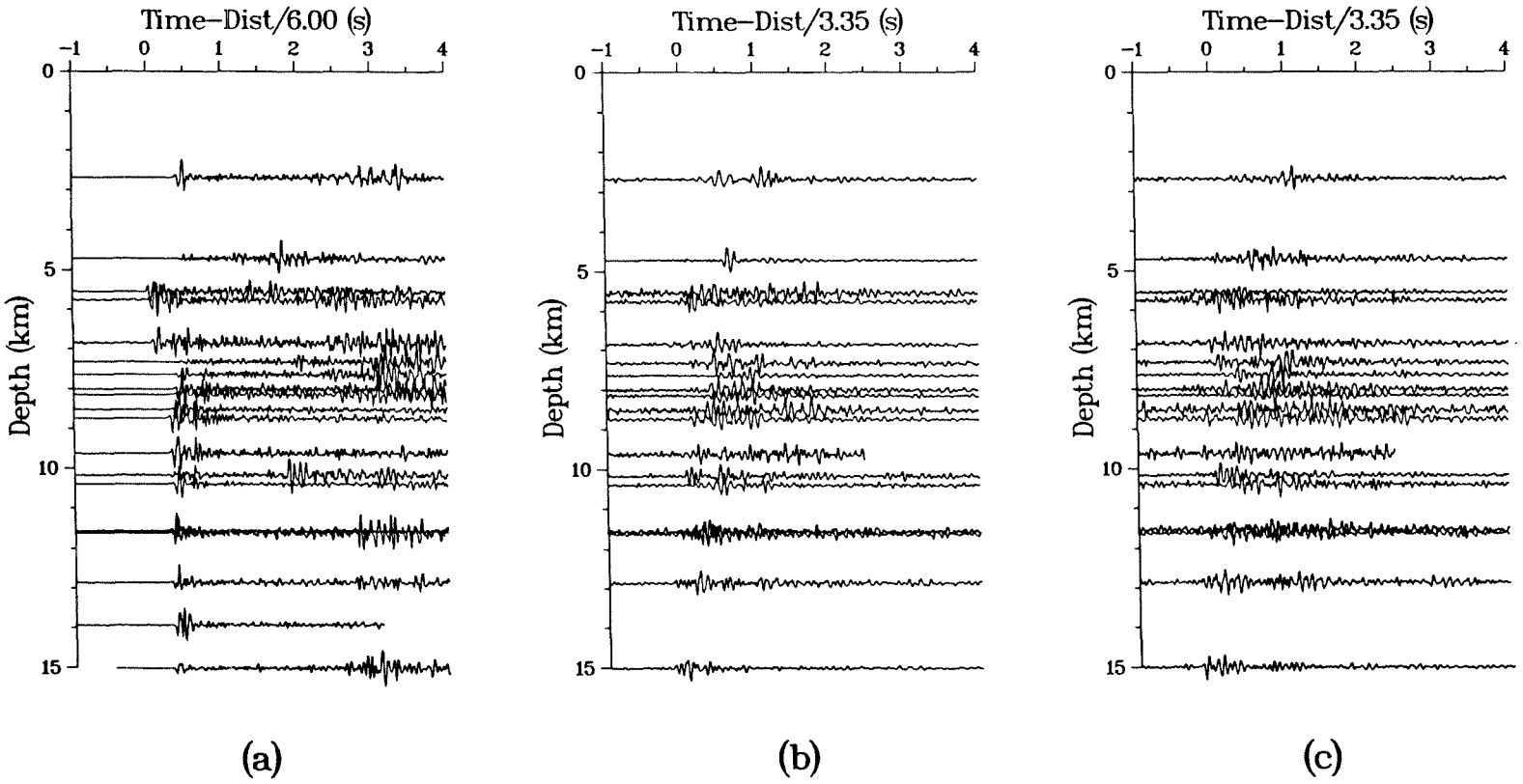

Fig. 3. Vertical hypocentral profiles for the (a) vertical and (b) and (c) two horizontal components of the borehole seismometer.

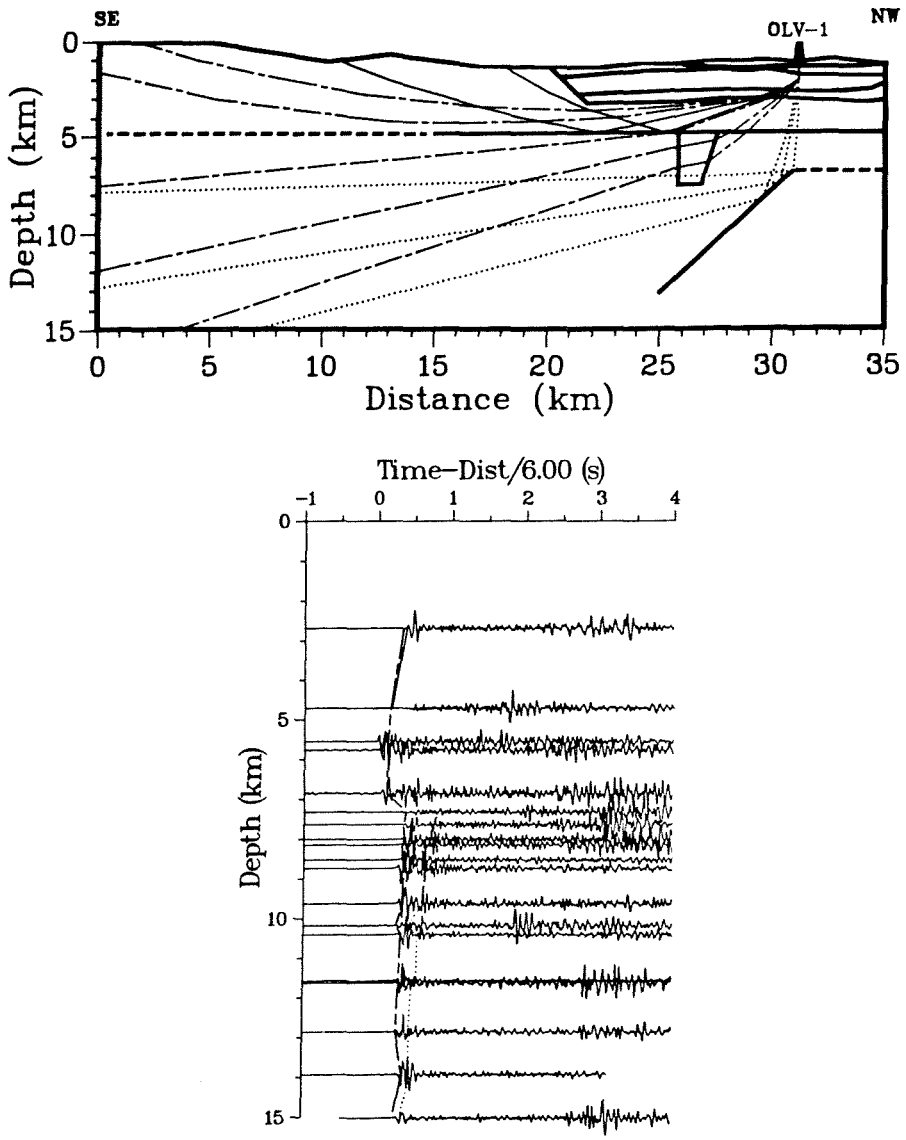

Fig. 4. Ray diagram and travel time curves for vertical component VHP. Phases shown in ray diagram and calculated travel times shown on VHP record section are direct *P* wave (dashed), reflected off horizontal interface (solid), and reflected off dipping interface (dotted). Jagged appearance of calculated travel time curves due to differences in hypocentral distance.

section overlain by the travel times calculated through the velocity model. The somewhat jagged appearance of these travel time curves is due to the variation in distance to the hypocenters.

Several important aspects of the velocity model are immediately obvious. The first of these is the midcrustal low-velocity body at 5 km depth beneath the southern portion of the resurgent dome within the caldera. This region accounts for the 0.4-s delay seen in the direct *P* wave arrival. The remaining ray paths of the direct wave allow upper bounds to be placed upon the vertical extent of the low-velocity body because these paths do not exhibit the same delay. A "normal" crustal velocity of 6.1 km/s was used both to match the observed undelayed arrivals in this study and for consistency with previous work [*Leutgert and Mooney*, 1985; *Hill et al.*, 1985*c*].

A second major feature of the model is the steeply dipping reflector located almost directly beneath well OLV-1 and dipping down to the southeast. This reflector gives rise to the second arrival noted on the vertical component record section. The low-velocity body is also important for this phase, delaying shallower events and thus causing the change in slope for this arrival between 7 and 8.5 km. The bottom of the low-velocity body is well constrained by the delayed and undelayed portions of the reflected phase.The top of this reflector cannot be directly determined but can be inferred by the abrupt truncation of the reflected phase at about 7 km on the record section indicating a significant change in slope of the reflector. Unfortunately, the lack of rays penetrating the region below the reflector makes it impossible to determine the velocity of this region. The relative amplitude of the reflection, however, indicates a sizable impedance contrast at this boundary.

Last, we have added a horizontal layer at 4.9 km depth to the basic model of *Hill et al.* [1985*c*]. This was included to help match the shallow (<5 km) first arrivals. Reflections off this boundary arrive at essentially the same time as the direct phase. The paucity of data at the shallower depths makes

this boundary very poorly constrained, and it could easily be a change in gradient rather than a sharp boundary as illustrated.

S Wave Velocity Model

The horizontal component VHPs (Figures 3*b* and 3*c*) exhibit many of the same characteristics as were seen on the vertical component but with one significant difference. In addition to two arrivals that appear to correspond to those noted in the vertical component VHP, a small-amplitude arrival now appears near the time expected for an undelayed, direct *S* wave arrival. Shortly after this arrival, however, a significantly larger-amplitude phase comes in with an arrival time near that expected for a direct *S* wave arrival delayed by an amount proportional to the delay seen in the direct *P* wave arrivals for the same depth range. Although the small-amplitude arrival could be a converted or reflected compressional wave, the geometry of the travel time curve for this phase, the lack of a boundary in the *P* wave model to give rise to an arrival at this time, and the comparable amplitude of this arrival and the direct shear wave arrival on the vertical component led us to model this as a pure shear wave. For this reason, it was decided to model the first arrival on the horizontal VHPs as a reflection undelayed by the low-velocity body in the deeper parts of the section, the second, larger-amplitude arrival as the direct shear wave, and the third arrival as another reflection. Other possible phases, such as the prominent arrival approximately 0.5 s behind the initial shear arrival at the shallowest depths, were not of sufficient depth range to be modeled with any degree of confidence.

The initial model for the shear wave velocities was derived by dividing the compressional wave velocities by the factor 1.73, while preserving the same subsurface structure. The final shear wave velocity model, along with the horizontal VHPs and computed travel times, are shown in Figure 5. Several of the shear velocities had to be modified from those derived from the compressional data to adequately fit the observed data.

The crustal structure affects the shear waves in much the same way as the compressional waves, delaying the direct wave below 7 km, and the reflected phases at shallower depths. An additional reflector essentially parallels the deeper reflector seen in the compressional velocity model and provides the earliest shear wave arrival from the deeper events. The velocity for the region between the two reflectors is poorly defined due to the trade-off between the thickness of the layer and the velocity. Based on the compressional wave velocity model and the amplitude of the earliest shear wave arrival, the velocity of 3.70 km/s was used.

The modeling of the vertical and horizontal component VHPs has provided a reasonable image of the crust beneath Long Valley caldera. Figure 6 shows the final model derived with both the compressional and shear velocities noted and the differences between the two velocity structures displayed. Velocities are accurate to about ±0.1 km/s, based on travel time variations noted during the modeling. This model is not a unique picture, however, as demonstrated by the uncertainty of the 3.70 km/s velocity mentioned above. A unique model would require reversing the source-receiver geometry, with the earthquakes to the north and the buried receiver to the south. Unfortunately, there are essentially no earthquakes north of the southern portion of the caldera, so this critical experiment cannot be performed. In addition, the other travel paths, such as diffracted phases, could give rise to the delayed phases noted on the VHPs.

While the midcrustal low-velocity body is well constrained in vertical extent by the various ray paths, it is not well constrained in horizontal dimensions. The same time delay can be derived if we allow some (<0.5 km due to geometrical considerations) lateral extension of the body with a simultaneous increase of the internal compressional (<1.37 km/s) and shear (<0.72 km/s) velocities.

It is also important at this point to discuss the error introduced into the final velocity model due to the inaccuracies in the locations of the hypocenters, especially the focal depths. Errors in the focal depths from Table 1 range up to 1.5 km. To examine the effect of these errors on the vertical component VHP, several sections were plotted that varied the depths of the events by either adding or subtracting (chosen randomly) the maximum depth error for that event as shown in Table 1. An example of such a section is shown in Figure 7*b*. In general, the overall shapes of the travel time curves were preserved, especially the abrupt delays due to the shallow low-velocity body. The depth at which this delay occurred, however, shifted by as much as ±1.2 km corresponding to a similar shift in the depth to the top of the low-velocity body. As a whole, then, it appears that errors in the boundary depths determined by ray tracing are closely related to errors in the focal depths, and to a lesser degree the epicenter locations and origin times, of the events used in constructing the sections. In any case, it is important to plot several sections with the errors introduced, as in Figure 7, to determine how dependent any derived models are to these uncertainties.

As can be inferred from the previous discussion, the model derived in this study does contain some inherent ambiguities. Nevertheless, our numerical experiments with a variety of models and consistency with the results of previous investigators provide strong evidence for the existence of the major features of the model (i.e., the separate low-velocity body at 5 km depth and the deeper reflectors).

DISCUSSION

The modeling of both the compressional and shear wave velocities now permits some discussion of crustal composition based not only on modeled changes in the velocity but also on the relative changes in the compressional and shear velocity (the V_p/V_s ratio). A case in point is the low-velocity body at 5 km depth. Here a compressional wave velocity decrease of 46%, a shear velocity decrease of 53%, and an increase in the V_p/V_s from 1.67 for the surrounding material to 1.91 for the low-velocity body are all inferred.

Studies have shown that a variety of factors can lead to changes in velocities, including mineral composition [*Kern and Richter*, 1981], partial melting [*Mavko*, 1980; *O'Connell and Budiansky*, 1977; *Birch*, 1969], temperature [*Murase and McBirney*, 1973; *Spencer and Nur*, 1976], pressure [*Christensen and Fountain*, 1975; *Spencer and Nur*, 1976], and fluid content [*Nur and Simmons*, 1969; *Spencer and Nur*, 1976; *O'Connell and Budiansky*, 1977]. Only two of these mechanisms, fluid content and partial melting, are capable of producing velocity decreases on the order of those modeled at the appropriate depths.

Although the presence of pore fluids and vapor have not

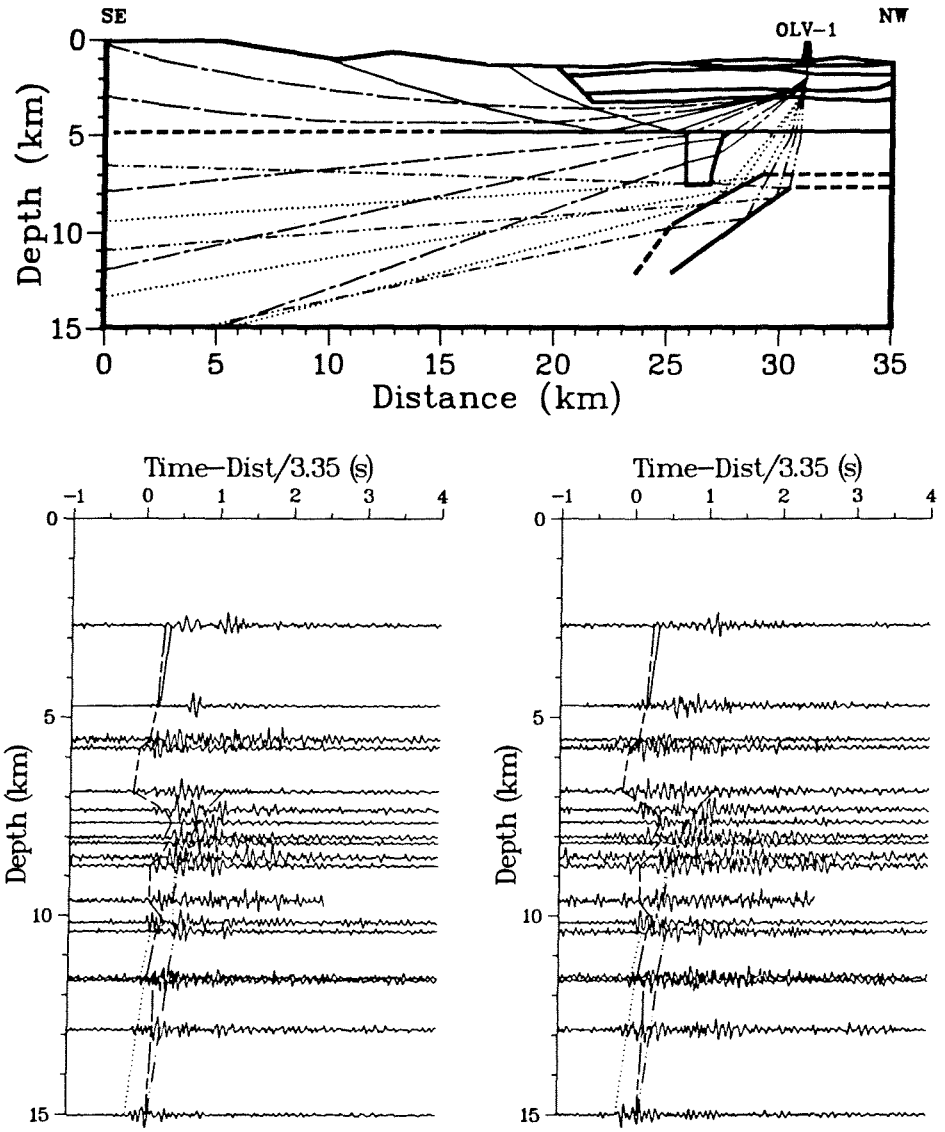

Fig. 5. Ray diagram and travel time curves for horizontal component VHPs. Phases shown in ray diagram and calculated travel times shown on VHP record sections are direct S wave (dashed), reflected off horizontal interface (solid), reflected off upper dipping interface (dotted), and reflected off lower dipping interface (dash-dotted). Jagged appearance of calculated travel time curves due to differences in hypocentral distance.

been seen to produce quite the velocity decrease modeled, the possible variations in the model discussed above still allow this to be a plausible explanation. *Spencer and Nur* [1976] observed V_p decreases of the order of 15% at temperatures of only 350°C at 1 kbar, primarily due to effects of the liquid-vapor transition of the pore fluids. At higher temperatures, however, the effect on the compressional velocity is much greater than on the shear velocity leading to a noticeable decrease in the V_p/V_s ratio, the opposite of what is observed in the model. Thus only partial melting can explain both the magnitude of the velocity decrease and the increase in the V_p/V_s ratio.

Estimates of the percentage of partial melt using observed velocity decreases have been made for the Yellowstone region [*Lehman et al.*, 1982] based on theoretical derivations by *O'Connell and Budiansky* [1977] and *Mavko* [1980]. A 30% compressional velocity decrease was calculated to result from a 9% to 30% partial melt fraction depending on the technique used and the assumptions made. A similar range of partial melt fraction is applicable to the low-velocity body in this study with the comparable 46% compressional velocity decrease modeled. It is not known, however, whether the low-velocity region represents a zone of essentially homogeneous material of constant melt fraction, such as a small magma body, or an area of both high and low melt fractions in geometries below the resolving power of the wavelengths used, as might be expected if the zone is in reality highly intruded by small dikes.

Another region of interest is the layer between the two deeper reflectors shown in the shear wave model where the shear velocity has increased, but the compressional velocity has remained constant (Figure 6). This effect has not been observed as a result of changes in temperature or pressure, or of partial melting. It most likely reflects a change in composition of either the rock itself or the pore fluids. The anomalous layer thus appears to be a zone of alteration of the country rock, or perhaps actual replacement of the country rock by solidified magma.

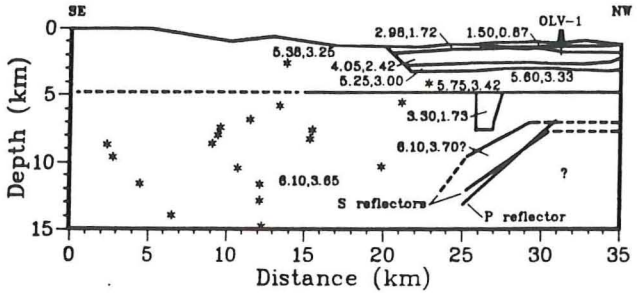

Fig. 6. Final velocity structure showing compressional (first) and shear (second) wave velocities (in kilometers per second) as well as differences in the P and S velocity structures in the deeper part of the model. Earthquake hypocenters used in the study are again shown as asterisks.

The final geologic interpretation of the section is displayed in Figure 8. Again, the interpretation of the near-surface structure is taken from *Hill et al.* [1985c]. The caldera fill is composed of layers of sediments, postcaldera volcanics, and the thick layer of Bishop Tuff. In the crystalline basement the more subtle changes in velocity and velocity gradients, such as that modeled at 4.9 km depth, are interpreted as resulting from changes due to pressure and temperature variations, and not from compositional changes.

The two magma bodies shown correspond to the small low-velocity body and the region below the lowest modeled reflector in Figure 6. Although no rays penetrated into this deeper region, the degree of velocity contrast, indicated by the relative amplitude of the reflected phase, and the results of other investigators [*Sanders*, 1984; *Kissling et al.*, 1984] support the interpretation of this reflector as the top of a large magma chamber. This deeper chamber may be the source of the shallow magma body through a feeder conduit that cannot be resolved with the present data set. The shallow body is pictured as a fairly homogeneous body but, as mentioned before, may actually be a zone that has been permeated by small intrusions. A zone of altered or replaced country rock forms a "rind" around the deeper magma chamber to account for the difference in P and S wave velocities.

The location of seismic anomalies that we found agrees well with previous models for structure beneath Long Valley (Figure 8). Previous seismic studies did not resolve a separation of the two magma chambers; however, the inflation model of *Rundle and Whitcomb* [1984] indicated two centers of injection that correspond well to the two magma bodies interpreted in this study.

The magnitude of the velocity decrease inferred for the shallow magma body would under many circumstances be coincident with a large density decrease that would give rise to a significant gravity anomaly. If, however, we are dealing with a zone of partial melting as indicated by the V_p/V_s ratio, the velocity decrease may be of a substantially larger percentage than the density change. For example, laboratory results from *Murase and McBirney* [1973] for a rhyolite obsidian, a rock type similar to what might be expected beneath Long Valley, showed a decrease in compressional wave velocity of 50% over a range of temperatures from 800°C to 1200°C with a corresponding decrease in density of only 2% over the same temperature range. Any significant density contrast for the magma zones would have to arise from compositional differences. Assuming a density contrast between a rhyolitic magma and the surrounding granitic basement of -0.4 g/cm^3, the gravity anomaly for the shallow low-velocity body calculated using the method of *Talwani et*

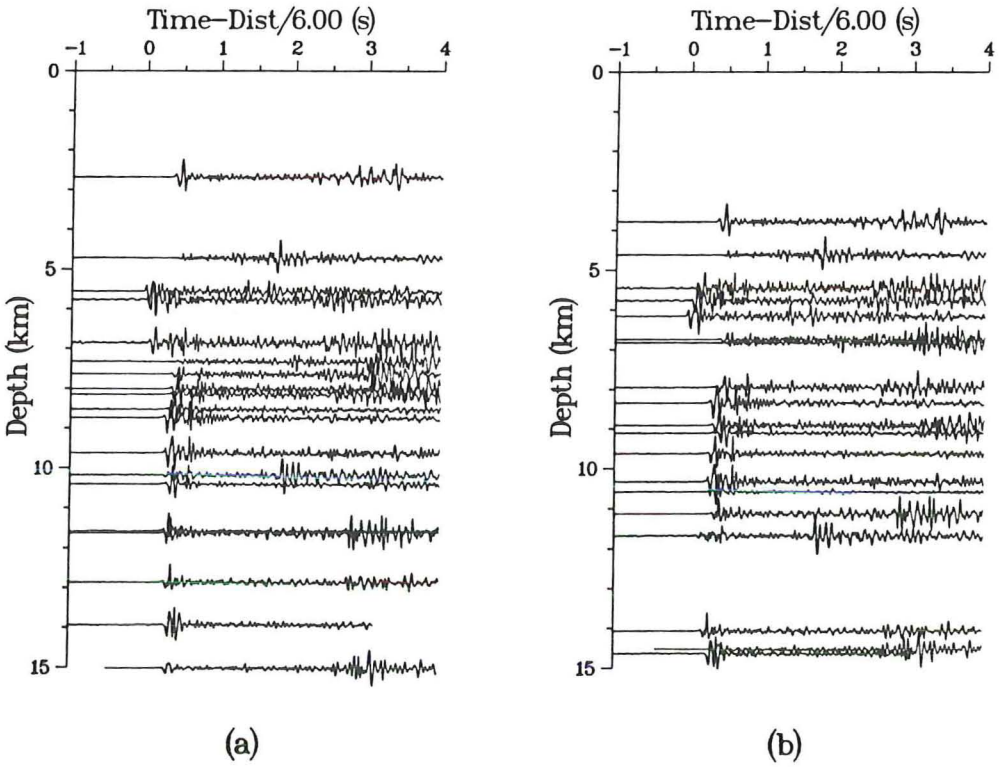

Fig. 7. Comparison of vertical-component VHP record sections (*a*) without depths shifted and (*b*) with depths shifted by the maximum estimated errors in depth.

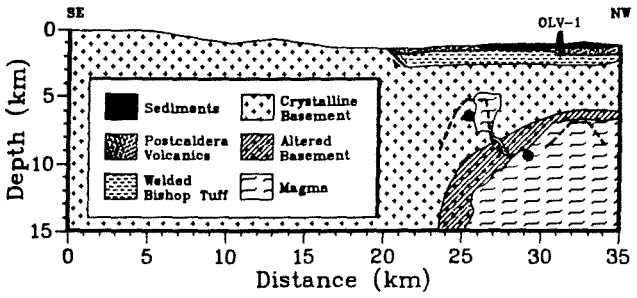

Fig. 8. Idealized geologic structure beneath Long Valley. Heavy dashed lines show outline of magma cupolas defined by *Sanders* [1984]. Solid dots represent centers of inflation modeled by *Rundle and Whitcomb* [1984].

al. [1959] is of a magnitude less than 5 mGal, an anomaly easily masked by variations in the near-surface caldera fill. The deeper magma body would give rise to a larger anomaly, but the extent of such an anomaly would cover the same region as the 50-mGal anomaly attributed to the caldera fill [*Kane et al.*, 1976] and would be difficult to separate out. Until more detailed gravity work is undertaken, gravity results can neither confirm nor dispute the model presented here.

Finally, although the cross section shown is modeled as two dimensional, the range in azimuths from 130° to 180° actually provides an estimate of 6-km minimum width for the smaller magma body. The deeper magma chamber is too near the receiver for any meaningful width to be estimated.

CONCLUSIONS

The use of borehole seismometers and the display of the records in vertical hypocentral profiles have both proved to be valuable in the exploration of this complicated volcanic terrain. The use of the downhole sensors in conjunction with the earthquake sources avoided almost entirely the more highly attenuating near-surface layers and preserved the high-frequency content of the waveforms, especially in the horizontal component. This allowed the shear wave velocity structure to be analyzed, which proved to be crucial in the interpretation of the crustal structure.

The vertical hypocentral profiles were found to be an extremely useful way of displaying the earthquake data and have great potential in areas with sufficient seismic activity, favorable hypocentral distribution, and reliable hypocenter locations. The VHPs can penetrate deeper into the crust than most conventional surface or borehole seismic techniques yet still contain the high-frequency information needed for good resolution of the subsurface. By using various azimuthal ranges, three-dimensional structure can be obtained. In addition, field operations are minimal for the amount of information obtained, requiring only one recorder. Used in conjunction with surface seismic surveys, the crust can be imaged quite well to significant depths.

Interpretation of the Long Valley data has revealed the existence of two separate magma bodies beneath the resurgent dome. The first of these is located with a depth to top of about 3.7 km beneath the surface at the southern end of the resugent dome and the second, larger body is at 5.5 km depth beneath the northern end of the resurgent dome. In addition, a rind of altered or replaced country rock was seen surrounding the larger magma body.

Acknowledgments. The authors would like to thank Tom Henyey and Egill Hauksson for their help in collecting and cataloging the data. This project supported by the U.S. Department of Energy under contract DE-AC04-76DP00789 to Sandia National Laboratories.

REFERENCES

Bailey, R. A., G. B. Dalrymple, and M. A. Lanphere, Volcanism, structure, and geochronology of Long Valley caldera, Mono County, California, *J. Geophys. Res.*, *81*, 725–744, 1976.

Birch, F., Density and composition of the upper mantle: First approximation as an olivine layer, in *The Earth's Crust and Upper Mantle*, *Geophys. Monogr. Ser.*, vol. 13, edited by P. J. Hart, pp. 18–36, AGU, Washington, D. C., 1969.

Cerveny, V., I. A. Molotkov, and I. Psencik, *Ray Method in Seismology*, 214 pp., Charles University Press, Prague, 1977.

Christensen, N. I., and D. M. Fountain, Constitution of the lower continental crust based on experimental studies of seismic velocities in granulite, *Geol. Soc. Am. Bull.*, *86*, 227–236, 1975.

Deemer, S. J., Seismic reflection profiling in the Long Valley caldera, California: Data acquisition, processing, and interpretation, M.S. thesis, Univ. of Wyo., Laramie, 1985.

Deemer, S. J., M. C. Humphreys, R. A. Johnson, and S. B. Smithson, Structure of the Long Valley caldera interpreted from seismic reflection data, *Eos Trans. AGU*, *66*, 301–302, 1985.

Hill, D. P., Structure of the Long Valley caldera from seismic refraction experiments, *J. Geophys. Res.*, *81*, 745–753, 1976.

Hill, D. P., R. A. Bailey, and A. S. Ryall, Active tectonic and magmatic processes beneath Long Valley caldera, eastern California: An Overview, *J. Geophys. Res.*, *90*, 11,111–11,120, 1985*a*.

Hill, D. P., R. E. Wallace, and R. S. Cockerham, Review of evidence on the potential for major earthquakes and volcanism in the Long Valley–Mono Craters–White Mountains regions of eastern California, *Earthquake Predict. Res.*, *3*, 571–594, 1985*b*.

Hill, D. P., E. Kissling, J. H. Leutgert, and U. Kradolfer, Constraints on the upper crustal structure of the Long Valley–Mono Craters volcanic complex, eastern California, from seismic refraction measurements, *J. Geophys. Res.*, *90*, 11,135–11,150, 1985*c*.

Kane, M. F., D. R. Mabey, and R. L. Brace, A gravity and magnetic investigation of the Long Valley caldera, Mono County, California, *J. Geophys. Res.*, *81*, 754–762, 1976.

Kern, H., and A. Richter, Temperature derivatives of compressional and shear wave velocitites in crustal and mantle rocks at 6 kbar confining pressure, *J. Geophys.*, *49*, 47–56, 1981.

Kissling, E., W. L. Ellsworth, and R. S. Cockerham, Three-dimensional structure of the Long Valley Caldera, California region by geotomography, Proceedings of a Conference on Active Tectonic Magmatic Processes Beneath Long Valley Caldera, Eastern California, *U.S. Geol. Surv. Open File Rep.*, *84-939*, 188–220, 1984.

Lee, W. H. K., and J. C. Lahr, HYPO71 (revised): A computer program for determining hypocenter, magnitude and first motion pattern of local earthquakes, *U.S. Geol. Surv. Open File Rep.*, *75-311*, 113 pp., 1975.

Lehman, J. A., R. B. Smith, M. M. Schilly, and L. W. Braile, Upper crustal structure of the Yellowstone caldera from seismic delay time analysis and gravity correlations, *J. Geophys. Res.*, *87*, 2713–2730, 1982.

Luetgert, J. H., and W. D. Mooney, Crustal refraction profile of the Long Valley caldera, California, from the January 1983 Mammoth Lakes earthquake swarm, *Bull. Seismol. Soc. Am.*, *75*, 211–221, 1985.

Mavko, G. M., Velocity and attenuation in partially molten rocks, *J. Geophys. Res.*, *85*, 5173–5189, 1980.

Murase, T., and A. R. McBirney, Properties of some common igneous rocks and their melts at high temperatures, *Geol. Soc. Am. Bull.*, *84*, 3563–3592, 1973.

Murphy, W. J., E. Renaker, M. Robertson, A. Martin, and P. Malin, The 1985 Mammoth wide-angle seismic reflection survey, *Eos Trans. AGU*, *66*, 960, 1985.

Nur, A., and G. Simmons, The effect of saturation on velocity in low porosity rocks, *Earth Planet. Sci. Lett.*, *7*, 183–193, 1969.

O'Connell, R. J., and B. Budiansky, Viscoelastic properties of fluid-saturated cracked solids, *J. Geophys. Res.*, *82*, 5719–5735, 1977.

Rundle, J. B., and J. H. Whitcomb, A model for deformation in Long Valley, California, 1980–1983, *J. Geophys. Res.*, *89*, 9371–9380, 1984.

Rundle, J. B., et al.; Seismic imaging in Long Valley, California, by surface and borehole techniques: An investigation of active tectonics, *Eos Trans. AGU*, *66*, 194–200, 1985.

Rundle, J. B., C. R. Carrigan, H. C. Hardee, and W. C. Luth, Deep drilling to the magmatic environment in Long Valley caldera, *Eos Trans. AGU*, *67*, 490–491, 1986.

Ryall, A., and F. Ryall, Attenuation of *P* and *S* waves in a magma chamber in Long Valley caldera, California, *Geophys. Res. Lett.*, *8*, 557–560, 1981.

Sanders, C. O., Location and configuration of magma bodies beneath Long Valley, California, determined from anomalous earthquake signals, *J. Geophys. Res.*, *89*, 8287–8302, 1984.

Spencer, J. W., and A. M. Nur, The effects of pressure, temperature, and pore water on velocities in Westerly granite, *J. Geophys. Res.*, *81*, 899–904, 1976.

Steeples, D. W., and H. M. Iyer, Low-velocity zone under Long Valley as determined from teleseismic events, *J. Geophys. Res.*, *81*, 849–860, 1976.

Talwani, M., J. L. Worzel, and M. Landisman, Rapid gravity computation for two-dimensional bodies with application to the Mendicino fracture zone, *J. Geophys. Res.*, *64*, 49–59, 1959.

G. J. Elbring and J. B. Rundle, Geophysics Division 1541, Sandia National Laboratories, Albuquerque, NM 87185.

(Received April 21, 1986;
revised July 25, 1986;
accepted August 6, 1986.)